Mansoura Engineering Journal

Volume 46 | Issue 1 Article 20

3-17-2021

Numerical Simulation of Buffeting Wind Forces on Cable Stayed Bridge.

Mohamed Abou El Saad
Emeritus professor in Determent of Structural Engineering, Faculty of Engineering, Mansoura University,
naguib2005@yahoo.com

Youssif Aggag
Emeritus professor in Determent of Structural Engineering, Faculty of Engineering, Mansoura University,
youssefagag@gmail.com

Ahmed Abd-Elsamea Khedr
Structural Engineering Department , Faculty of Engineering, Mansoura University, Mansoura, Egypt.,
ahmedgamal1991@mans.edu.eg

Recommended Citation

Abou El Saad, Mohamed; Aggag, Youssif; and Abd-Elsamea Khedr, Ahmed (2021) "Numerical Simulation of Buffeting Wind Forces on Cable Stayed Bridge.," *Mansoura Engineering Journal*: Vol. 46 : Iss. 1 , Article 20.
Available at: https://doi.org/10.21608/bfemu.2021.157319

Mansoura University
Faculty of Engineering
Mansoura Engineering Journal

Numerical Simulation of Buffeting Wind Forces on Cable Stayed Bridge

M. Naguib, *Y. Agag* and A. G. Khedr

KEYWORDS:

Cable stayed bridge; wind load; algorithm of simulation; time history; buffeting force.

***Abstract*— The numerical methods are widely adopted tool for simulation of wind histories. The most accurate technique is the wind tunnel test, but it is not the most economical option. Therefore, a lot of researches are concerned with developing those methods to be more accurate, applicable, and to save executed time of analysis. This paper is concerned with comparing two algorithms for simulation of stochastic stationary Gaussian processes. These algorithms are autoregressive method (AR) and spectral representation method (SR). For the implementation of the simulation methods, a MATLAB program is built for the two algorithms. The application of both methods is carried for using a cable stayed bridge having 670 m as a main span to study a set of points along the deck. The comparison between obtained results for both simulations is proposed. The statistical properties are calculated to compare and assess the results of both methods accurately. It is noticed that the simulated auto/cross-correlation functions of the simulated wind forces in two methods have good conformity with the target functions. Otherwise, SR method is more accurate than AR method, but the executed time in SR method is more than AR method. The research also, applied the accurate method to generate wind speeds for a cable stayed bridge to calculate the buffeting force.**

I. INTRODUCTION

RECENTLY, with the remarkable development in the use of cable bridges with large spans, wind effects become more paramount. Hence, the analysis of wind induced buffeting of large span bridges is considered necessary and cannot be disregarded. The stochastic vibration theory based on frequency domain encounter several complications in nonlinear wind induced structural response, so the time domain analysis method usually used to compute the nonlinear response of long span bridges under wind load with sufficient accuracy.

Wind velocity is indispensably considered in studying buffeting analysis of structures such as towers, tall building, and cable stayed and suspension bridges. The most accurate method especially for bridges to form wind velocity model is the wind tunnel test but it is not the most economical option for design stage for any structure. Therefore, it is significant to study the wind simulation by numerical methods.

Monte Carlo simulation is a well-established technique in wind engineering and is becoming a fundamental tool for the design of complex and important wind-excited structures. This technique generates sample functions of the stochastic processes. The generated sample functions must accurately describe the probabilistic characteristics of the corresponding stochastic processes, that may be either stationary or non-stationary, homogeneous or nonhomogeneous, one-

Received: (28 October, 2020) - Revised: (22 February, 2021) - Accepted: (25 February, 2021)

M. Naguib, Emeritus professor in Department of Structural Engineering, Faculty of Engineering, Mansoura University, Mansoura, Egypt.

Y. Agag, Emeritus Associate professor in Department of Structural Engineering, Faculty of Engineering, Mansoura University, Mansoura, Egypt.

***Corresponding Author** A.G. Khedr, Teaching assistant of structural analysis and mechanics, Structural Engineering Department, Faculty of Engineering, Mansoura University, Mansoura, Egypt, (e-mail Ahmedgamal1991@mans.edu.eg.)*

(Ser. No. Bfemu -2010-1065)

dimensional or multi-dimensional, one-variate or multi-variate and Gaussian or non-Gaussian. [1]

There are many algorithms for simulation of stochastic stationary/non-stationary Gaussian processes can be classified primarily into two categories [2] as shown in Fig.1:

1. Algorithms relied on the digital filters, which are autoregressive (AR) and moving average (MA) algorithms and their combination, autoregressive moving average (ARMA) algorithm.
2. Algorithms relied on summation of trigonometric functions with random phase angle such as spectral representation method (SR).

Shinozuka [3] and [4] was the first person presented an efficient method of simulating multivariate, multidimensional and non-stationary processes based on summation of cosine functions with random frequency and random phase angles (as called wave super position method). Yang [5], mentioned that the application of fast Fourier transform (FFT) technique to SR method is used to improve the computational efficiency. He also, proposed a formula to simulate random envelope processes. Shinozuka(1974) [6] adding the (FFT) technique to multidimensional process. Shinozuka and Levy (1977) [7] have described a procedure to simulate wind fluctuating part in two dimensional acting on the surface of paraboloidal antenna. Deodatis and Shinozuka (1989) [8] used the stochastic waves to simulate seismic ground motion and introduced the concept of double-indexing of frequencies. Deodatis(1996) [9] presented algorithm generates ergodic sample functions in the sense that the temporal cross-correlation matrix of each and every generated sample function is identical to the corresponding target, when the length of the generated sample function is equal to one period (the generated sample functions are periodic).

To improve efficiency and accuracy of the spectral method, a lot of researches were carried out. Cao et al (2000) [10] developed the algorithm of simulation by assuming that the mean wind is constant along the bridge span, which improve the efficiency of Cholesky's decomposition. Recently, Ding et al.[11] proposed very effective simulation algorithm form using the Fourier-Stieltjes integral of spectral representation, Huang et al.[12] Separated the phase from power spectrum density matrix to improve the efficiency of Cholesky's decomposition, Chen et al.[13] used the inverse fast Fourier transform to propesed a new efficient algorithm for generating short term time histories and Gao et al (2019) [14] proposed a modified spectral representation method to simulate non-Gaussian random vector process considering wave-passage effect.

The AR method is one of simulation techniques which uses linear filters. Iwatani (1982) [15] proposed the use of an AR model (multidimensional AR process) to simulate multiple wind velocities. Iannuzzi and Spinelli (1987) [16] compared the methods of simulating both single and multiple wind velocities. Huang and Chalabi (1995) [17] used an AR model to produce non-stationary Gaussian random processes to simulate the wind velocity and a Kalman filter to estimate the parameters of the AR model. Kumar and Mohammadian (1996) [18] proposed the auto-regressive (AR) model to simulate wind loads for mono slope roofs of various geometries. Facchini (1996) [19] used a hybrid model to simulate wind velocity and mentioned that the coefficients of AR model which can be calculated directly from the spectral density of the target process without using of Yule-Walker equations. Li and Dong (2001) [20] presented a matrix method to determine the parameters of the AR model without the iteration which effectively avoided the accumulative errors in the simulation. Poggi et al. (2003) [21] used an AR model to simulate wind speed in Corsica and compared the results with an experimental data to check the simulated wind speed.

The main object of this paper is to compare between simulation wind speed methods (AR and SR) based on the accuracy, executed time of generation and their applicability to use. A cable stayed bridge with span 670m as main span has been used for the comparison. Then, the simulation of load on the selected cable stayed bridge is applied using the appropriate method.

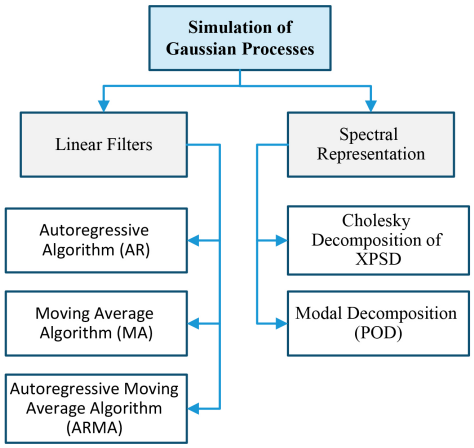

Fig. 1. Diagram of methods used for simulating Gaussian processes.

II. THE AUTOREGRESSIVE METHOD

A model which depends only on the previous histories of the processes to predict wind velocities is called an autoregressive method (AR). The AR method is a representation of a type of random process. The AR method filters white noise and transforms it into a signal with a specified variance and autocovariance function [22].

To generate a stochastic process u(t) with zero mean and variance $\sigma_u{}^2$, the method for transforming white noise which used by Box and Jenkins [23], can be described by the following equation:

$$u(t) = \gamma(B).a(t) \tag{1}$$

A. *Mean wind speed profile*

In strong wind conditions, the mean wind profile due to extra-tropical cyclones and monsoons can be expressed by the accurate mathematical expression which called "logarithmic law". The logarithmic law was originally derived for the

turbulent boundary layer on a flat plate, however it has been found to be valid in an unmodified form for strong winds in the atmospheric boundary layer near the ground [24]. The "logarithmic law" can be expressed as:

$$\bar{U}(z) = \frac{1}{k} u_* \ln\left(\frac{z}{z_0}\right) \quad (2)$$

$$u_* = \frac{U(10)}{2.5 \ln\left(\frac{10}{z_0}\right)} \quad (3)$$

B. Power spectral density function

The power spectral density function, which is shortened usually to wind spectrum, is used to describe frequency distribution of the fluctuating velocity components and define the random nature of wind. Kaimal spectrum [25] is used to describe longitudinal, lateral and vertical velocity fluctuations as follow:

$$S_u(z,n) = \frac{200 * {u_*}^2 * z}{U_Z * \left(1 + 50\left(\frac{z*n}{U_Z}\right)\right)^{\frac{5}{3}}} \quad (4)$$

$$S_V(z,n) = \frac{15 * {u_*}^2 * Z}{U_Z * \left(1 + 9.5\left(\frac{z*n}{U_Z}\right)\right)^{\frac{5}{3}}} \quad (5)$$

$$S_w(z,n) = \frac{3.36 * {u_*}^2 * Z}{U_Z * \left(1 + 10\left(\frac{z*n}{U_Z}\right)^{\frac{5}{3}}\right)} \quad (6)$$

The cross-correlation matrix is given by:

$$R^o(\tau) = \begin{bmatrix} R^0_{11}(\tau) & R^0_{12}(\tau) & \dots & R^0_{1N}(\tau) \\ R^0_{21}(\tau) & R^0_{22}(\tau) & \dots & R^0_{2N}(\tau) \\ \dots & \dots & \dots & \dots \\ R^0_{N1}(\tau) & R^0_{N2}(\tau) & \dots & R^0_{NN}(\tau) \end{bmatrix} \quad (7)$$

The diagonal terms of cross-correlation matrix, $R^0_{jk}(\tau)$: j=1,2….,n, represent the autocorrelation functions and the off-diagonal elements, $R^0_{jk}(\tau)$: j=k=1,2…..,n: j ≠ k represent the cross-correlation functions of the stochastic process.

The cross-spectral density matrix of random fluctuations is given by:

$$S^o(\omega) = \begin{bmatrix} S^0_{11}(\omega) & S^0_{12}(\omega) & \dots & S^0_{1N}(\omega) \\ S^0_{21}(\omega) & S^0_{22}(\omega) & \dots & S^0_{2N}(\omega) \\ \dots & \dots & \dots & \dots \\ S^0_{N1}(\omega) & S^0_{N2}(\omega) & \dots & S^0_{NN}(\omega) \end{bmatrix} \quad (8)$$

The diagonal elements of the cross-spectral density matrix, $S^0_{jk}(\omega)$: j=1,2…..,n represent the power spectral density function of the stochastic process and the off-diagonal elements $S^0_{jk}(\omega)$: j=k=1,2…..,n: j ≠ k correspond to the cross-spectral density functions.

In homogeneous turbulence flow, the imaginary part (quadrature-spectrum) is negligible. The reports on the quadrature-spectrum of the wind turbulence in the atmospheric boundary layer are very scanty and has been reported in Simiu and Scanlan [26]. In general, the co-spectrum $S^C_{ij}(n)$ between two processes u_i and u_j defined as:

$$S_{ij}(n) = \sqrt{S_{ii}(n)\, S_{jj}(n)}\; e^{-f} \quad (9)$$

The following expression for the coherence function for two points on a plane perpendicular to the mean wind direction was proposed by Davenport.[27]

$$coh_{ij}(n) = e^{-f} \quad (10)$$

$$f = \frac{2n\sqrt{C_y^2\left(Y_j - Y_i\right)^2 + C_z^2\left(Z_j - Z_i\right)^2}}{U(Z_i) + U\left(Z_j\right)} \quad (11)$$

The elements of cross-correlation matrix are related to the corresponding elements of the cross-spectral density matrix through Wiener-Khintchine transformation, τ is the time lag and ω is the frequency.

$$S^0_{jk}(\omega) = \frac{1}{2\pi} \int_{-\infty}^{\infty} R^0_{jk}(\tau) e^{-i\omega\tau}\, d\tau, \qquad j,k = 1,2,\dots,n \quad (12)$$

$$R^0_{jk}(\tau) = \int_{-\infty}^{\infty} S^0_{jk}(\omega) e^{-i\omega\tau}\, d\omega, \qquad j,k = 1,2,\dots,n \quad (13)$$

C. Implementation of Iwatani method

In the following, a step by step procedure for the generation of multiple wind histories by the method proposed by Iwatani [15] can be summarized as follows:

Step 1 Select the mean wind speed *U (10)* at 10m height and the roughness length z_0. Then, compute the mean shear velocity u_* using eqn.(3) and the mean wind speed $U(z)$ at the required height z using eqn.(2).

Step 2 Calculate the cross-correlation matrix *K*K* $R_u(m\Delta t)$, $m = 0,1,\dots,M$. According to eqn.(13), the cross correlation $R^{ij}_u(\tau)$ between two processes u_i and u_j at a time lag τ given by the following two equations, (14) and (15):

$$R_u^{ij}(\tau) = \int_{n1}^{n2} \sqrt{S_i(z_i,n).\ S_j(z_j,n)} * e^{-f} * \cos(2\pi n\tau)\, dn \quad (14)$$

(In a plane perpendicular to the wind direction) and

$$R_u^{ij}(\tau) = \int_{n1}^{n2} \sqrt{S_i(z_i,n).\ S_j(z_j,n)} * e^{-f} * \cos(2\pi n\tau + \tau')\, dn \quad (15)$$

(In the along to the wind direction)

Where e^{-f} is known as the narrow-band cross-correlation and f is given by eqn.(11).

And τ' is the value of the additional lag given by:

$$\tau' = 2\frac{(x_i - x_j)}{U(z_i) + U(z_j)} \quad (16)$$

The spectral density function $S_u(z,n)$can be determined according to Kaimal spectrum, using eqns. (4), (5) and (6) for longitudinal, lateral and vertical velocity fluctuation respectively, n is the frequency. The initial and the cut-off frequencies of the spectrum $n_1$and n_2 are equal to $2/T$ and 2.5 Hz, respectively, and T is the total sample of duration. The constants c_y and c_z are known as "the exponential decay coefficients", in most cases c_y and c_z may be taken as 8 [28].

Step 3 Obtain the inverse of the matrix $R_u(0)$ and estimate the normalized matrix $r_u(m\Delta t)$, using eqn.(17).

$$r_u(m\Delta t) = R_u(m\Delta t) * R_u^{-1}(0) \quad (17)$$

Step 4

Construct and store the matrix r which has the vector $\tilde{r}$ in the $(M+1)^{th}$column.
For example, with m=4.

$$r = \begin{bmatrix} r_u(0) & r_u^T(\Delta t) & r_u^T(2\Delta t) & r_u^T(3\Delta t) \\ r_u^T(\Delta t) & r_u(0) & r_u^T(\Delta t) & r_u^T(2\Delta t) \\ r_u^T(2\Delta t) & r_u^T(\Delta t) & r_u(0) & r_u^T(\Delta t) \\ r_u^T(3\Delta t) & r_u^T(2\Delta t) & r_u^T(\Delta t) & r_u(0) \end{bmatrix}$$

$$\tilde{r} = \begin{bmatrix} r_u(\Delta t) \\ r_u(2\Delta t) \\ r_u(3\Delta t) \\ r_u(4\Delta t) \end{bmatrix}$$

Step 5 Solve the linear system of eqn.(18), for the unknowns ϕ^T using Gauss-Jordan elimination method.

$$r.\tilde{\phi} = \tilde{r} \quad (18)$$

For an order of $M = 4$ parameters, the eqn.(18) can be rewritten as.

$$\begin{bmatrix} r_u(0) & r_u^T(\Delta t) & r_u^T(2\Delta t) & r_u^T(3\Delta t) \\ r_u^T(\Delta t) & r_u(0) & r_u^T(\Delta t) & r_u^T(2\Delta t) \\ r_u^T(2\Delta t) & r_u^T(\Delta t) & r_u(0) & r_u^T(\Delta t) \\ r_u^T(3\Delta t) & r_u^T(2\Delta t) & r_u^T(\Delta t) & r_u(0) \end{bmatrix} \begin{bmatrix} \phi_1^T \\ \phi_2^T \\ \phi_3^T \\ \phi_4^T \end{bmatrix} = \begin{bmatrix} r_u(\Delta t) \\ r_u(2\Delta t) \\ r_u(3\Delta t) \\ r_u(4\Delta t) \end{bmatrix} \quad (19)$$

Where ϕ is an autoregressive matrix at time lag Δt. The elements of r, $\tilde{r}$ and ϕ are $K * K$ matrix.

Step 6 Transpose the M matrices ϕ_m^T.

Step 7 Calculate the matrix r_N, using eqn.(20), and calculate the cross-correlation matrix of random shocks R_N using eqn.(21).

$$r_N = I - [\phi_1, \phi_2 \dots \dots \phi_M] * [r_u(\Delta t), r_u(\Delta t), \dots\dots, r_u(M\,\Delta\, t)]^T \quad (20)$$

$$R_N = r_N.R_u(0) \quad (21)$$

Step 8 Determine the lower triangular matrix L. Given a symmetric positive definite matrix R, the lower triangular matrix L can be determined using the recursive formulae given below such that $R = LL^T$. The diagonal elements are found from eqn.(22) :

$$L^{ii} = \sqrt{\left[R^{ii} - \sum_{m=1}^{i-1} (L^{im})^2\right]} \quad (22)$$

The off-diagonal elements (j < i) from eqn.(23):

$$L^{ij} = \frac{1}{L^{jj}}\left[R^{ij} - \sum_{m=1}^{i-1} L^{im}L^{jm}\right] \quad (23)$$

For each time step

Step 9 Generate the set of k random numbers with normal distribution, zero mean and unit variance, using an appropriate routine.

Step 10 Transfer the uncorrelated random process n(t), having a Gaussian distribution with zero mean and unit variance to the correlated random process $N(t)$ by using the following equation:

$$\mathrm{N(t)} = \mathrm{L.\,n(t)} \tag{24}$$

$$\mathrm{n(t)} = [\mathrm{n_1(t), n_2(t), \dots\dots, n_k(t)}]^{\mathrm{T}} \tag{25}$$

Step 11 Calculate the new estimate of the processes, $u^i(t), i = 1,2,3, \dots\dots, K$ where the immediate value of the processes $u^i(t), i = 1,2,3, \dots\dots, K$ is expressed as a finite aggregate of M previous values of each process $u^i(t), i = 1,2,3, \dots\dots, K$ as:

$$\mathrm{u^i(t)} = \sum_{\mathrm{m=1}}^{\mathrm{M}} \sum_{\mathrm{j=1}}^{\mathrm{k}} \phi_{\mathrm{m}}{}^{\mathrm{ij}} \mathrm{u^j(t - m\Delta t)} + \mathrm{N^i(t)} \tag{26}$$

Step 12 Compute the instantaneous values of the total processes, V(t), using the following equation:

$$V(z,t) = \mathrm{U(z)} + u(z,t) \tag{27}$$

III. Spectral Representation (SR) Method

The algorithm which is proposed by Ding et al. [11], transformed the frequency domain to the time domain in the simulation technique. It can be expressed as:

$$u_j(t) = \sqrt{2\Delta f} \sum_{l=0}^{N-1} \sum_{m=1}^{n} \left|H_{jm}(f_l)\right| \cos[2\pi f_{ml} t + \emptyset_{ml} + \theta_{jm}(f_l)] \tag{28}$$

f_{ml} can be calculated by the following equation:

$$f_{ml} = l\Delta f + \frac{m}{n}\Delta f \tag{29}$$

$$\Delta f = \frac{f_{up}}{N} \tag{30}$$

$$\theta_{jm}(f_l) = \tan^{-1}\left\{\frac{\mathrm{Im}\left[H_{jm}(f_l)\right]}{\mathrm{Re}\left[H_{jm}(f_l)\right]}\right\} \tag{31}$$

Im $[H_{jm}(f_l)]$ and Re$[H_{jm}(f_l)]$ are the imaginary and real parts of $H_{jm}(f_l)$ respectively.
$\theta_{jm}(f_l)$ is neglected because of the imaginary part is ignored.

The periodic time of the generated sample function can be calculated according to the following equation:

$$T = \frac{n}{\Delta f} = \frac{nN}{f_{up}} \tag{32}$$

The value of time step Δt can be expressed as:

$$\Delta t = \frac{1}{2f_{up}} \tag{33}$$

A. Numerical Illustration for Ding algorithm

In the following, a step by step procedure for the generation of multiple wind histories by the method proposed by [11] can be summarized as follows:

Step 1 Select the mean wind speed *U (10)* at 10m height and the roughness length z_0. Then, compute the mean shear velocity u_* using eqn. (3), and the mean wind speed $U(z)$ at the required height z using eqn. (2).

Step 2 Calculate the cross-spectral density matrix at each frequency by using eqn.(12)and coherence eqn.(13)

Step 3 Calculate the lower triangular matrix by decomposed cross spectral density matrix using cheloskey decomposition into the following format:

$$S_p(f) = H(f)H^T(f) \tag{34}$$

$H(f)$ is the lower triangular matrix can be expressed as:

$$H(f) = \begin{bmatrix} H_{11}(f) & 0 & \dots & 0 \\ H_{21}(f) & H_{22}(f) & \dots & 0 \\ \vdots & \vdots & \ddots & \vdots \\ H_{n1}(f) & H_{n2}(f) & \dots & H_{nn}(f) \end{bmatrix} \tag{35}$$

Step 4 Generate random phase angles which are uniformly distributed over the interval $[0,2\pi]$.
Calculate f_{ml} and Δt according to eqns.(29) and (33) respectively.

Step 5 Generate time history of wind turbulent component by using eqn.(28)

Step 6 Compute the instantaneous values of the total processes, V(t), using eqn.(27).

As illustrated in Fig. 2, diagram show how method applying in MATLAB and can be summarized the equation of this algorithm into two matrix being multiplied and then aggregated over the all frequency steps and can be expression the eqn.(28) in matrix format as follow:

$$u = \sqrt{2\Delta f}\,[H][B] \tag{36}$$

$$\mathbf{H}=\begin{bmatrix} H_{1,1}(f_1) & H_{2,1}(f_1) & \cdots & H_{1,n}(f_1) \\ H_{2,1}(f_1) & H_{2,2}(f_1) & \cdots & H_{2,n}(f_1) \\ \vdots & \vdots & \ddots & \vdots \\ H_{n,1}(f_1) & H_{n,2}(f_1) & \cdots & H_{n,n}(f_1) \\ H_{1,1}(f_2) & H_{2,1}(f_2) & \cdots & H_{1,n}(f_2) \\ H_{2,1}(f_2) & H_{2,2}(f_2) & \cdots & H_{2,n}(f_2) \\ \vdots & \vdots & \ddots & \vdots \\ H_{n,1}(f_2) & H_{n,2}(f_2) & \cdots & H_{n,n}(f_2) \\ \vdots & \vdots & \ddots & \vdots \\ H_{1,1}(f_{N_f}) & H_{2,1}(f_{N_f}) & \cdots & H_{1,n}(f_{N_f}) \\ H_{2,1}(f_{N_f}) & H_{2,2}(f_{N_f}) & \cdots & H_{2,n}(f_{N_f}) \\ \vdots & \vdots & \ddots & \vdots \\ H_{n,1}(f_{N_f}) & H_{n,2}(f_{N_f}) & \cdots & H_{n,n}(f_{N_f}) \end{bmatrix}$$

$$\mathbf{B}=\begin{bmatrix} \cos(2\pi f_1 t_1+\varphi_{1,1}) & \cos(2\pi f_1 t_2+\varphi_{1,1}) & \cdots & \cos(2\pi f_1 t_{N_t}+\varphi_{1,1}) \\ \cos(2\pi f_1 t_1+\varphi_{1,2}) & \cos(2\pi f_1 t_2+\varphi_{1,2}) & \cdots & \cos(2\pi f_1 t_{N_t}+\varphi_{1,2}) \\ \vdots & \vdots & \ddots & \vdots \\ \cos(2\pi f_1 t_1+\varphi_{1,n}) & \cos(2\pi f_1 t_2+\varphi_{1,n}) & \cdots & \cos(2\pi f_1 t_{N_t}+\varphi_{1,n}) \\ \cos(2\pi f_2 t_1+\varphi_{2,1}) & \cos(2\pi f_2 t_2+\varphi_{2,1}) & \cdots & \cos(2\pi f_2 t_{N_t}+\varphi_{2,1}) \\ \cos(2\pi f_2 t_1+\varphi_{2,2}) & \cos(2\pi f_2 t_2+\varphi_{2,2}) & \cdots & \cos(2\pi f_2 t_{N_t}+\varphi_{2,2}) \\ \vdots & \vdots & \ddots & \vdots \\ \cos(2\pi f_2 t_1+\varphi_{2,n}) & \cos(2\pi f_2 t_2+\varphi_{2,n}) & \cdots & \cos(2\pi f_2 t_{N_t}+\varphi_{2,n}) \\ \vdots & \vdots & \ddots & \vdots \\ \cos\left(2\pi f_{N_f} t_1+\varphi_{N_f,1}\right) & \cos\left(2\pi f_{N_f} t_2+\varphi_{N_f,1}\right) & \cdots & \cos\left(2\pi f_{N_f} t_{N_t}+\varphi_{N_f,1}\right) \\ \cos\left(2\pi f_{N_f} t_1+\varphi_{N_f,2}\right) & \cos\left(2\pi f_{N_f} t_2+\varphi_{N_f,2}\right) & \cdots & \cos\left(2\pi f_{N_f} t_{N_t}+\varphi_{N_f,2}\right) \\ \vdots & \vdots & \ddots & \vdots \\ \cos\left(2\pi f_{N_f} t_1+\varphi_{N_f,n}\right) & \cos\left(2\pi f_{N_f} t_2+\varphi_{N_f,n}\right) & \cdots & \cos\left(2\pi f_{N_f} t_{N_t}+\varphi_{N_f,n}\right) \end{bmatrix}$$

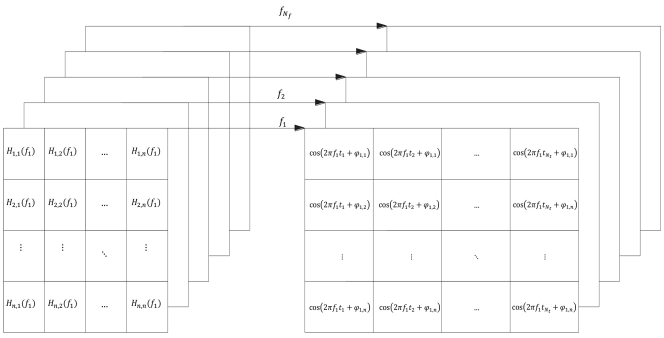

Fig.2: Diagram show how implementing wind velocity by spectral method in MATLAB.

IV. NUMERICAL EXAMPLE

An original version of a software tool for AR method was written by Naguib, M. [29] in FORTRAN language. Later, that program was rewritten as a MATLAB script. Also, for comparison purposes, another MATLAB script was written by the author for the implementation of SR method.

MATLAB software is used to implement the proposed method because, it has wide use of matrix calculations. By applying the previous steps using the MATLAB functions, the stochastic wind field on long span cable stayed bridges could be generated. Also, all statistical properties are done on the results to ensure its validity and conformity with the original data on which the program is based such as, spectrum and coherence.

The three-dimensional wind velocity field of along cable-stayed bridge with respect to the bridge directions are illustrated in Fig.3 and can be defined as:

$$\begin{aligned} U &= \bar{U}(z)+u(y,z,t) && 0<y\le L, 0<z\le H \\ v &= v(y,z,t) && 0<y\le L, 0<z\le H \\ w &= w(y,z,t) && 0<y\le L, 0<z\le H \end{aligned} \quad (37)$$

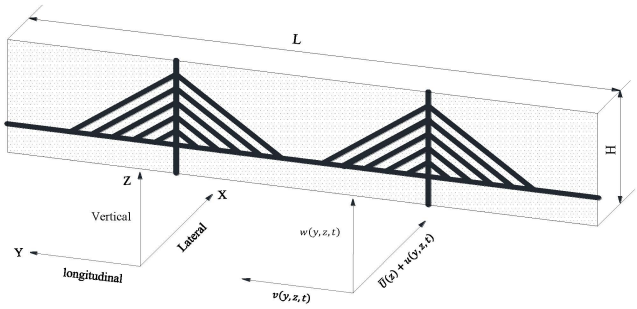

Fig. 3: Wind field of cable stayed bridge.

The artificial wind velocity field has been generated for the cable stayed bridge with a total span of 1270 m shown in Fig. Fig.4 using the two previously mentioned methods (i.e. AR and SR) to evaluate and compare the performance and efficiency of wind simulation techniques.

First of all, the model was idealized to a group of members connected at joints. Then, the wind velocity was calculated at each joint as shown in Fig.5.

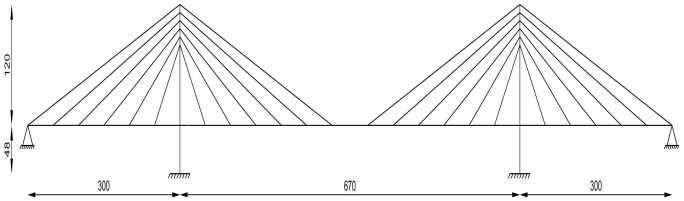

Fig. 4: Cable stayed bridge model (dimensions are given in m).

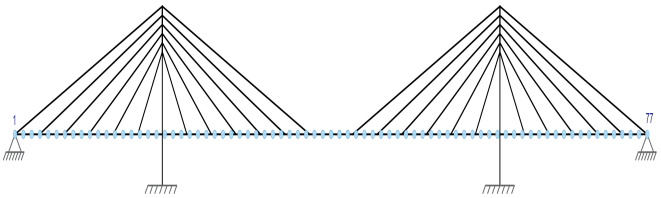

Fig. 5: Position of the simulation points.

The main data involved in the wind velocity simulation is tabulated in Table 1.

TABLE 1
VALUES OF INPUTTED DATA FOR GENERATION PROGRAM.

Height of the deck above ground	Z=60 m
Velocity of wind at 10m elevation	$U(10) = 18.8\ m/sec$
Ground roughness	$Z_0 = 0.08$ m
Upper cutoff frequency	$f_{up} = 2\ Hz$
Dividing number of frequencies	N=2048
Time interval	$\Delta t = 0.25\ sec$
Decay coefficient	$C_y = 10\ , C_z = 10$
No. of accuracy (any number ≥ 2)	NC=5
No. of autoregressive parameters (3:5)	ND=3
No. of processes (Time histories)	NP=77

V. BUFFETING FORCE

The buffeting forces are caused by the fluctuating part of wind velocity, which consists of the along wind component *u (x, t)* and vertical component *w (x, t)*. Buffeting of the bridge per unit span shown in Fig.6 [i.e., lift $L_b(t)$, drag $D_b(t)$, and pitching moment $M_b(t)$], can be expressed according to the quasi- steady theory as follows:

$$L_b = \frac{1}{2}\rho U^2 B\left[2C_L\frac{u(x,t)}{U} + (C_L' + C_D)\frac{w(x,t)}{U}\right] \quad (38)$$

$$D_b = \frac{1}{2}\rho U^2 B\left[2C_D\frac{u(x,t)}{U} + C_D'\frac{w(x,t)}{U}\right] \quad (39)$$

$$M_b = \frac{1}{2}\rho U^2 B^2\left[2C_M\frac{u(x,t)}{U} + C_M'\frac{w(x,t)}{U}\right] \quad (40)$$

$$C_L' = \frac{dC_L}{d\alpha}\ , C_D' = \frac{dC_D}{d\alpha}\ , C_M' = \frac{dC_M}{d\alpha} \quad (41)$$

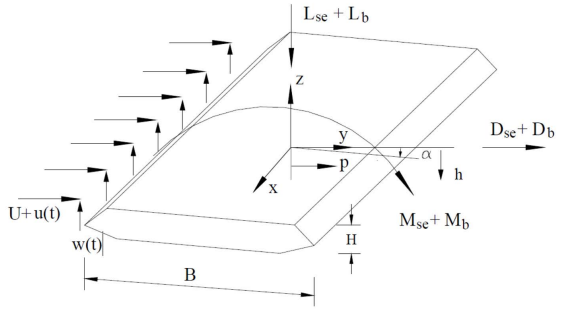

Fig. 6: Aerodynamic forces on bridge deck section.

This approach is most valid for small reduced frequency (or large reduced velocity) where the time taken for the flow to traverse the bridge deck is very short compared to the oscillation time. In this case, the effects of the motion of the deck are communicated rapidly to the flow region surrounding it. In another word, it is valid when disturbances in the flow have appreciably larger dimensions than the deck itself [30].

The description for buffeting forces, modified using the aerodynamic admittance functions as discussed by (Davenport (1962), Chen *et al* (2000)), are given as follows:

$$L_b = \frac{1}{2}\rho U^2 B\left[2C_L\chi_{Lbu}\frac{u(x,t)}{U} + (C_L' + C_D)\chi_{Lbw}\frac{w(x,t)}{U}\right] \quad (42)$$

$$D_b = \frac{1}{2}\rho U^2 B\left[2C_D\chi_{Dbu}\frac{u(x,t)}{U} + C_D'\chi_{Dbw}\frac{w(x,t)}{U}\right] \quad (43)$$

$$M_b = \frac{1}{2}\rho U^2 B^2\left[2C_M\chi_{Mbu}\frac{u(x,t)}{U} + C_M'\chi_{Mbw}\frac{w(x,t)}{U}\right] \quad (44)$$

Where $\chi_{Lbu}, \chi_{Lbw}, \chi_{Dbu}, \chi_{Dbw}, \chi_{Mbu}, \chi_{Mbw}$ are the aerodynamic admittance functions, which are functions of the reduced frequency and dependent on the geometrical configuration of the cross section of the bridge deck described by using Sears function which simplified by Liepmann is of the form:

$$|\chi(k)|^2 = \frac{1}{1+2\pi k} + \frac{1}{1+([\pi\omega B]/\bar{U})} \quad (45)$$

A. *Example for generating buffeting load*

An artificial wind velocity field has been generated for the Stonecutters bridge shown in Fig.7 by using (SR) method. The wind velocity field on the bridge deck is assumed to be composed of 231 wind velocity waves distributed along the deck, piers, and towers. The main data involved in the wind velocity simulation are as follows:
$\omega_{up} = 4\pi\ rad/sec$,$N = 1024$,$N_T = 2048$ and$\Delta t = .25\ sec$

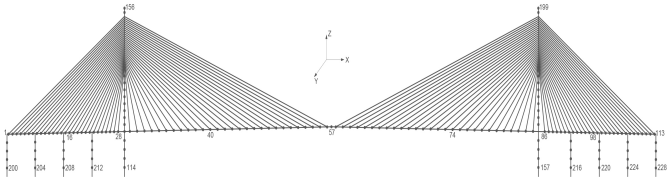

Fig. 7: Distribution of nodes corresponding to the generation of wind speed time series.

The wind turbulence characteristics identified for this study published by (Hui, Michael C H Ding, Q S Xu, Y L)[30] , included power wind spectra ,turbulence intensities, turbulence length scales and root coherences, for wind direction perpendicular to the bridge longitudinal axis, which are summarized as follows:
Von Karman models:

$$\frac{f.S_{uu}(f)}{\sigma_u^2} = \frac{4 \cdot \frac{L_u \cdot f}{U}}{\left[1 + 70.8 \cdot \left(\frac{L_u \cdot f}{U}\right)^2\right]^{5/6}} \quad (46)$$

$$S_{u_i u_i}(f, z_i) = \frac{I_u^2(z_i) \cdot U(z_i) \cdot 4 \cdot L_u(z_i)}{\left[1 + 70.8 \cdot \left(\frac{L_u(z_i) \cdot f}{U(z_i)}\right)^2\right]^{5/6}} \quad (47)$$

$$\frac{f.S_{vv,ww}(f)}{\sigma_{v,w}^2} = \frac{4 \cdot \frac{L_{v,w} \cdot f}{U}\left[1 + 755 \cdot \left(\frac{L_{v,w} \cdot f}{U}\right)^2\right]}{\left[1 + 283 \cdot \left(\frac{L_{v,w} \cdot f}{U}\right)^2\right]^{11/6}} \quad (48)$$

Turbulence intensities:

$$I_u = \frac{\sigma_u}{U_{10}(Z)} = 0.16 \cdot \left(\frac{10}{Z}\right)^{0.19}$$
$$I_v = 0.97 \cdot I_u$$
$$I_w = 0.54 \cdot I_u \quad (49)$$

Turbulence length scales:

$$L_i = L_{i50} \cdot \left(\frac{Z}{50}\right)^{0.60} \quad i = u, v, w$$
$$(L_{i50} = L_i \; at \; 50m \; level)$$
$$L_{u50} = 151\,m \;\; ; \;\; L_{v50} = 34\,m \;\; ; \;\; L_{w50} = 13\,m \quad (50)$$

Root coherence:

$$\sqrt{coh} = exp\left(-C \cdot \frac{D \cdot f}{U_{10}(Z)}\right) \quad (51)$$

TABLE 2
THE VALUES OF THE DECAY FACTOR $\boldsymbol{C}$ [30].

	Lateral Separation	Longitudinal Separation	Vertical Separation
Longitudinal Fluctuating Wind Component	8.0	2.0	9.1
Lateral Fluctuating Wind Component	4.0	4.0	5.5
Vertical Fluctuating Wind Component	4.7	4.0	4.0

VI. RESULTS OF SIMULATION AND DISCUSSION

Table 3 shows the statistical properties of wind histories at a group of point along the bridge. The result showed that: The difference between maximum and minimum simulated velocity in the two methods is about (2-20) %. The variance for the two methods gives closer results.

For the difficulty of showing the result of all joints on the bridge in the figures, two joints are selected. A group of figures will be presented to illustrate the results of both selected wind simulation methods. The first three figures (Fig.8, Fig.9 and Fig.10) represent the results of AR while the other three ones (Fig.11, Fig.12 and Fig.13) represent those of SR. Each figure consists of eight charts representing the wind velocity at a specific point and its statistical properties which is necessary for the assessment of the results and holding comparisons between the two methods` accuracy where : (a) is the time history of wind velocity at point 1, (b) is the time history of longitudinal velocity at point 9, (c) is the auto correlation function at point 1, (d) is the corresponding PSD function, (e) is the cross-correlation function at points 1 and 9, (f) is the corresponding cross-PSD function, (g) is the co-coherence function between point 1 and point 9, (h) is the probability density function at point 1.

By comparing the results of the charts (c) and (e) in the figures which shown the temporal and target auto-/cross-correlation functions of simulated wind velocities at selected points, It is noticed that the temporal auto-/cross-correlation functions of simulated wind velocities have good agreement with the target. Also, it is found that the results of the SR method have a better correlation with the target function than the other method. This note assured that SR method has more accuracy than that of AR method.

In the chart (d) in the figures, it is shown that there is a good agreement between the target and simulated power spectrum of the selected points in both methods.

In the chart (g) in the figures, it is noticed that the values of coherence from the simulated process almost fitted by the target of coherence function. Also, the values of the coherence function of processes simulated by AR method are less scattered than of it simulated by SR method about the target coherence.

In the chart (h) in the figures, it is appeared that the output of both methods for the selected points are fit to the normal distribution. As known, the real wind velocity is subjected to standard normal distribution in nature. Hence, the result of simulation methods might be considered satisfactory. The results of the two methods showed a great convergence in the distribution.

Buffeting force caused by fluctuating wind speed shown in Fig.14 and Fig.15, which is calculated by using unit admittance and sears function respectively. The SR method is applied to generate wind histories and calculate buffeting force. Both the Sears function and the unit admittance are used in the computation for the bridge deck to find the lower bound and the upper bound of the buffeting response.

TABLE 3

STATISTICAL PROPERTIES OF WIND HISTORIES AT A GROUP OF POINT.

Joint	SR									AR								
	Longitudinal			Cross			Vertical			Longitudinal			Cross			Vertical		
	Max	Min	Var.	Max	Min	Var.	Max	Min	Var.	Max	Min	Var.	Max	Min	Var.	Max	Min	Var.
1	17.72	-18.09	23.84	10.68	-10.63	8.39	4.78	-4.94	1.82	18.77	-14.96	20.87	11.44	-10.95	8.13	5.02	-4.87	1.91
4	19.88	-20.21	25.11	9.52	-9.74	8.53	4.82	-4.90	1.90	16.88	-16.04	22.33	11.51	-10.33	8.39	5.02	-5.55	1.85
5	17.74	-17.92	24.22	10.11	-10.10	8.59	4.65	-4.75	1.85	17.61	-17.01	23.20	9.67	-11.10	8.02	5.25	-4.51	1.87
8	18.31	-18.23	22.99	10.31	-10.31	8.24	4.76	-4.69	1.83	19.52	-18.39	23.92	10.18	-10.55	8.77	5.07	-4.63	1.87
9	19.37	-19.21	23.47	9.73	-9.66	8.17	5.01	-5.03	1.88	18.47	-18.89	22.34	10.57	-10.66	8.85	6.08	-5.25	1.89
15	18.10	-18.40	23.66	10.39	-10.42	7.96	4.51	-4.54	1.78	16.79	-17.72	24.68	12.51	-11.18	8.90	4.75	-4.94	1.73
16	16.50	-17.02	22.95	10.46	-10.55	7.68	5.52	-5.42	1.91	17.05	-20.20	24.83	9.89	-11.04	8.68	4.45	-4.45	1.72
17	16.78	-17.08	24.13	11.62	-11.63	7.95	5.46	-5.52	1.80	16.56	-18.64	24.95	11.47	-11.21	8.76	4.74	-4.53	1.75
22	17.14	-16.63	21.72	12.13	-12.07	8.49	5.15	-5.17	1.88	15.26	-16.33	23.76	10.41	-9.86	8.75	5.03	-4.94	1.86
23	18.56	-18.11	21.75	10.85	-10.62	8.45	4.90	-4.89	1.79	18.58	-18.62	24.86	10.76	-11.15	8.66	4.99	-5.61	1.84
35	17.72	-17.98	23.84	10.65	-10.53	7.86	4.23	-4.28	1.64	16.74	-15.80	24.35	10.76	-10.04	8.49	4.32	-4.53	1.75
36	17.60	-17.37	25.16	10.14	-10.22	7.97	4.28	-4.24	1.65	19.51	-15.65	24.79	11.09	-9.85	8.26	4.52	-5.00	1.70
37	19.29	-19.26	26.54	10.34	-10.37	7.96	4.86	-4.77	1.64	20.82	-17.32	24.89	10.74	-11.70	8.32	4.81	-4.34	1.82
38	16.97	-17.05	24.99	10.27	-10.36	8.09	4.88	-4.89	1.62	19.61	-16.45	24.67	11.73	-10.86	8.07	4.48	-4.77	1.87
46	15.90	-15.55	23.38	9.23	-9.32	8.20	4.38	-4.39	1.67	16.68	-15.21	24.07	11.57	-10.41	8.35	5.55	-4.75	2.00
47	16.96	-17.36	23.08	9.92	-9.91	8.31	4.78	-4.77	1.80	17.22	-14.59	23.35	9.61	-10.47	8.53	5.81	-5.08	1.95
48	17.13	-17.51	23.77	10.75	-10.75	8.41	4.75	-4.79	1.79	18.21	-16.39	24.65	11.28	-12.05	8.93	5.82	-6.50	1.93
49	16.45	-16.21	23.58	10.36	-10.40	8.53	4.66	-4.69	1.76	17.42	-18.47	23.81	12.08	-12.69	8.53	5.08	-5.07	1.87
50	16.03	-14.84	23.32	10.65	-10.48	8.46	5.08	-5.09	1.70	18.49	-16.94	24.24	9.67	-10.51	8.56	4.94	-4.82	1.86
51	15.87	-15.94	22.84	12.66	-12.49	8.29	5.46	-5.50	1.82	17.26	-17.93	23.02	10.47	-10.01	8.45	5.12	-6.26	1.92
52	15.68	-15.20	22.87	12.11	-12.41	8.37	4.81	-4.67	1.79	17.56	-15.68	22.35	11.95	-10.84	8.52	5.41	-4.93	1.88
58	18.83	-18.65	23.22	11.27	-11.23	8.08	4.63	-4.44	1.84	19.61	-16.84	25.36	11.38	-10.91	8.42	4.55	-4.73	1.74
59	19.32	-19.20	23.83	10.32	-10.60	8.09	4.74	-4.68	1.71	19.31	-16.83	25.06	11.00	-10.33	8.63	4.40	-4.72	1.70
60	18.28	-17.89	24.97	10.56	-10.82	8.25	4.64	-4.66	1.70	15.54	-15.99	25.89	9.94	-11.35	8.75	5.35	-5.12	1.77
66	16.23	-16.42	25.78	11.30	-11.30	8.10	4.63	-4.82	1.69	17.30	-16.06	25.16	10.71	-10.96	8.45	4.94	-4.97	1.85
67	17.87	-18.23	25.01	10.86	-11.03	8.37	5.43	-5.51	1.71	17.19	-15.88	25.18	11.27	-11.68	8.70	5.01	-5.04	1.86
68	17.22	-17.56	23.95	9.39	-9.63	7.89	5.22	-5.17	1.70	17.66	-15.73	24.63	12.28	-10.57	8.77	4.81	-4.43	1.85
69	19.06	-18.99	23.34	10.43	-10.50	7.67	4.65	-4.69	1.70	18.39	-14.57	24.01	10.38	-11.80	8.58	5.91	-5.41	1.94
70	17.02	-16.61	23.75	10.90	-10.85	8.18	4.47	-4.50	1.63	18.64	-15.79	22.43	10.76	-10.91	8.36	4.49	-5.29	1.85

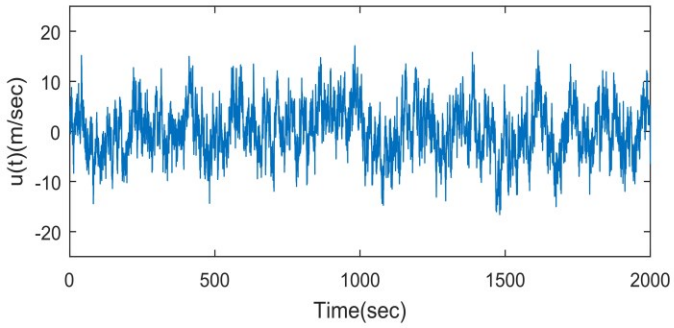

(a) Longitudinal velocities at point 1

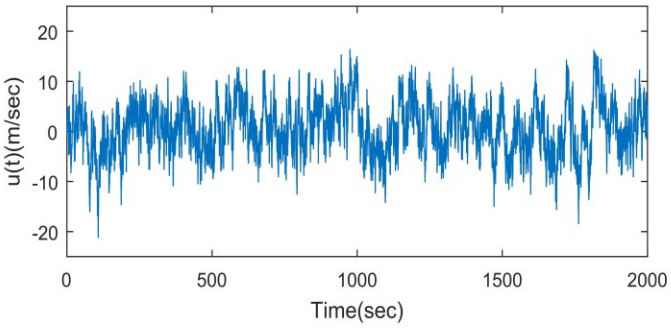

(b) Longitudinal velocities at point 9

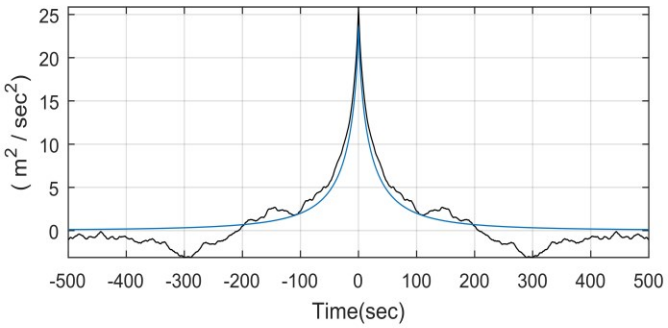

(c) Auto correlation function at point 1

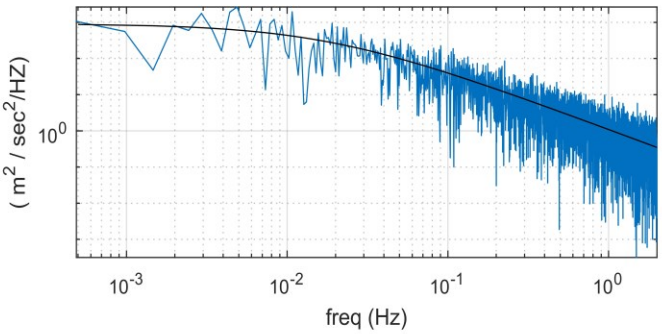

(d) PSD function at point 1

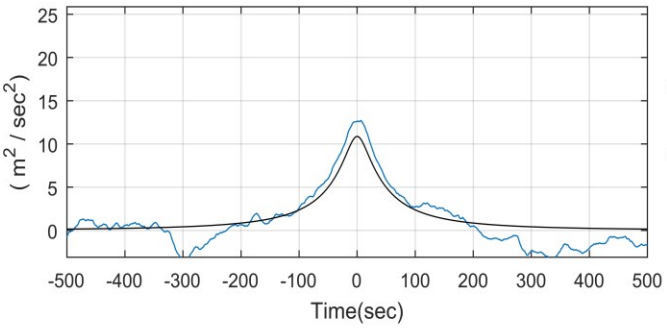

(e) cross-correlation function at points 1 and 9

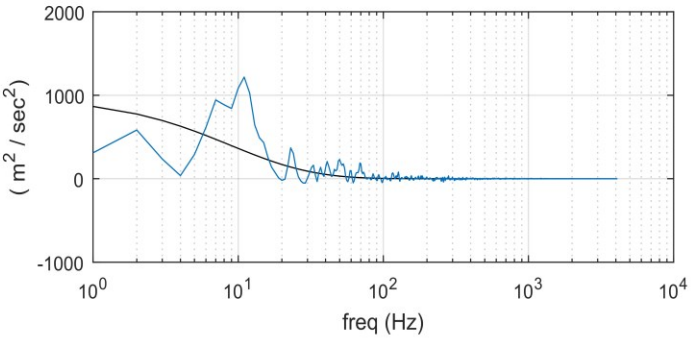

(f) cross-PSD function at points 1 and 9

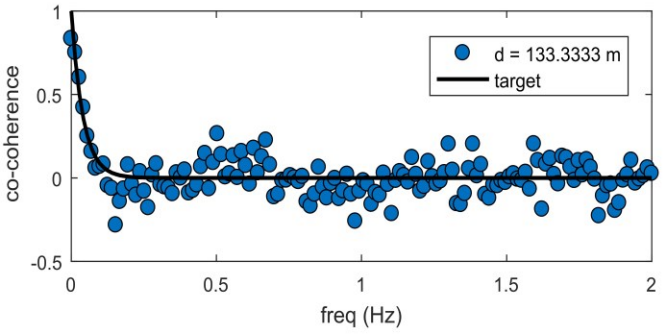

(g) Co-coherence function between points 1 and 9

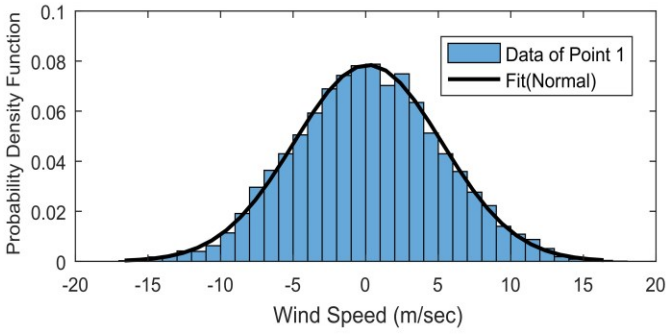

(h) probability density function at point 1

Fig. 8: Outputs of longitudinal wind speeds and their statistical analysis using AR-method.

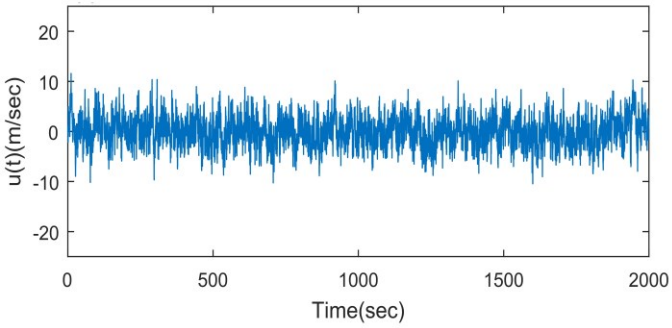

(a) Cross velocities at point 1

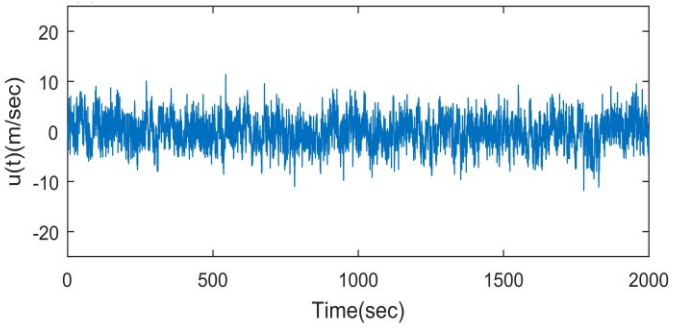

(b) Cross velocities at point 9

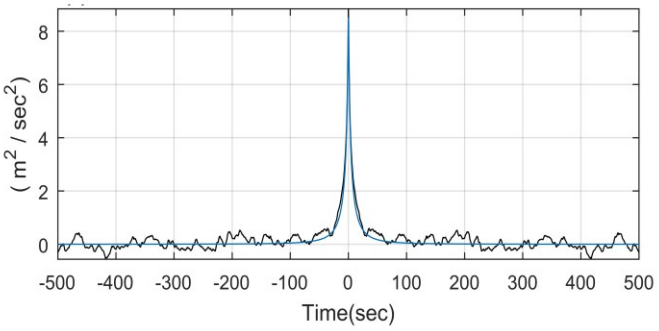

(c) Auto correlation function at point 1

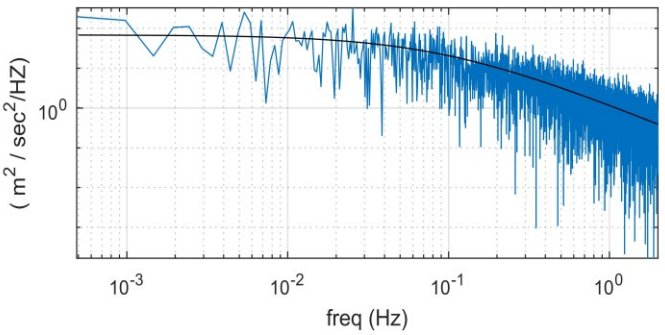

(d) PSD function at point 1

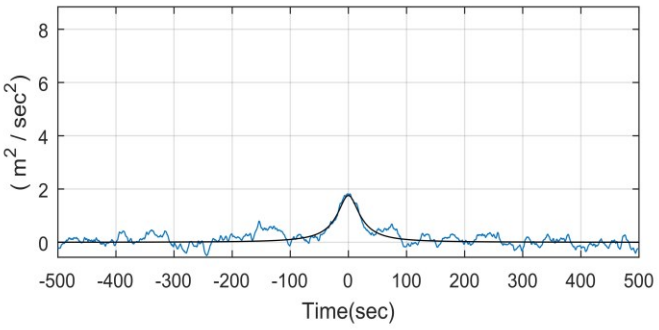

(e) cross-correlation function at points 1 and 9

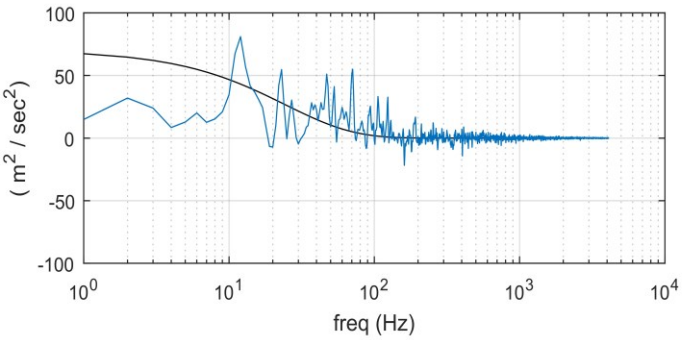

(f) cross-PSD function at points 1 and 9

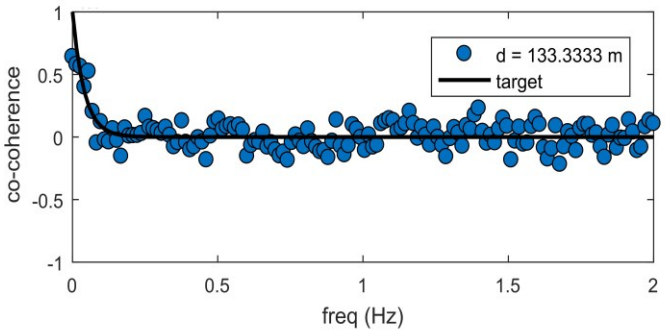

(g) Co-coherence function between points 1 and 9

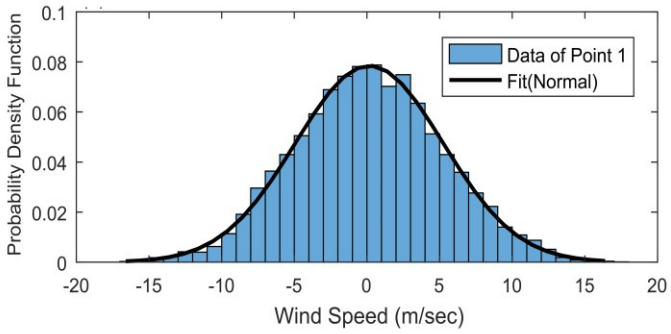

(h) probability density function at point 1

Fig. 9: Outputs of cross wind speeds and their statistical analysis using AR-method.

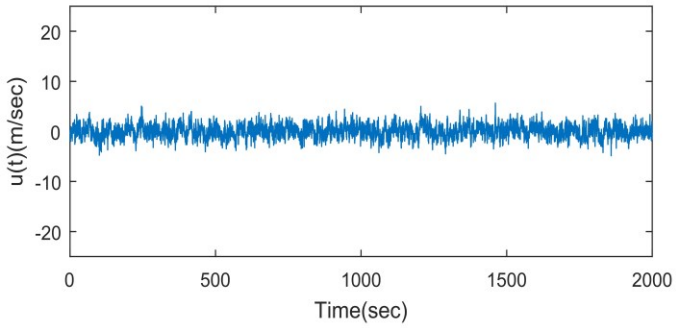

(a) Vertical velocities at point 1

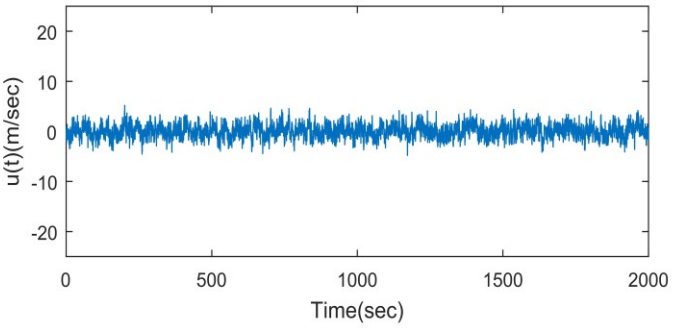

(b) Vertical velocities at point 9

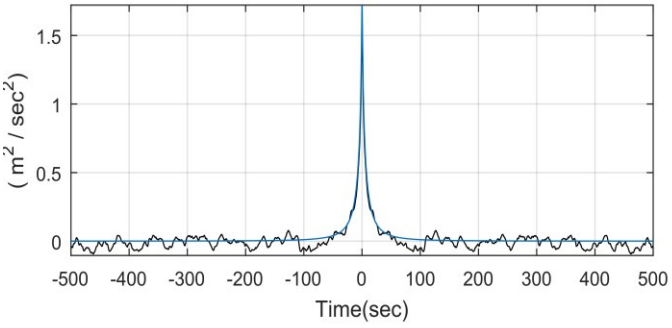

(c) Auto correlation function at point 1

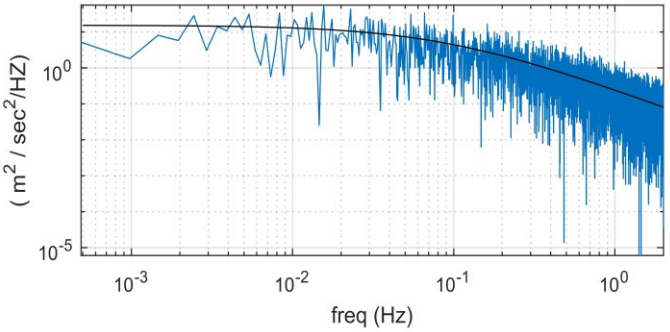

(d) PSD function at point 1

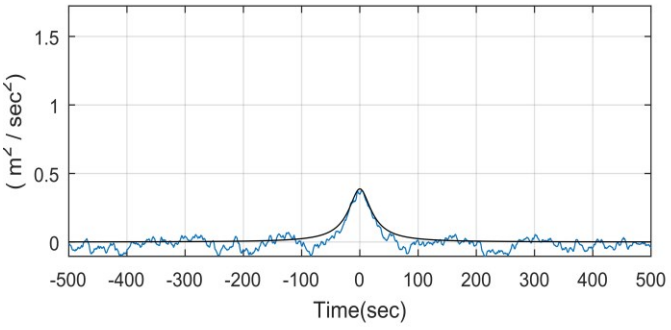

(e) cross-correlation function at points 1 and 9

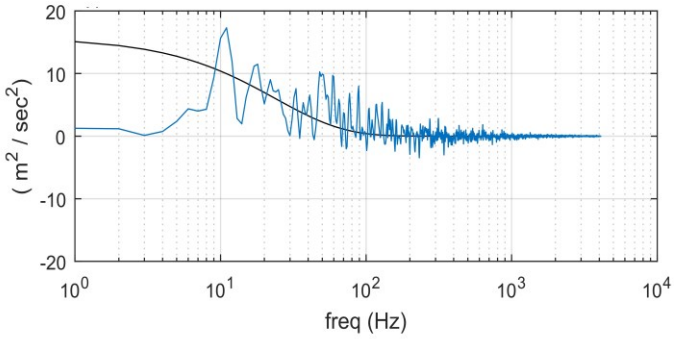

(f) cross-PSD function at points 1 and 9

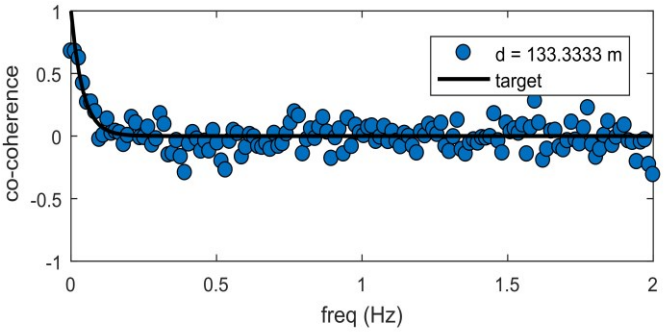

(g) Co-coherence function between points 1 and 9

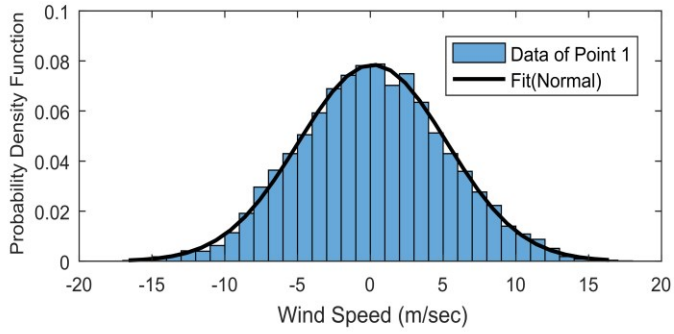

(h) probability density function at point 1

Fig. 10: Outputs of vertical wind speeds and their statistical analysis using AR-method.

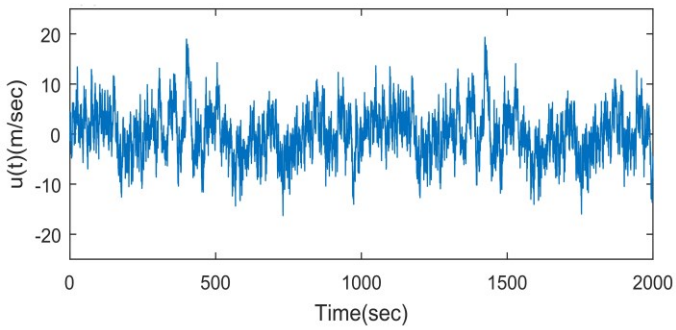

(a) Longitudinal velocities at point 1

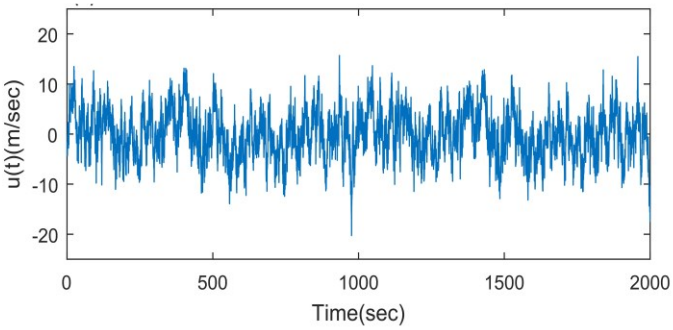

(b) Longitudinal velocities at point 9

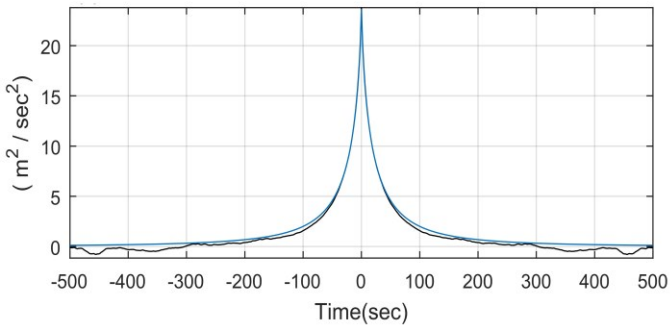

(c) Auto correlation function at point 1

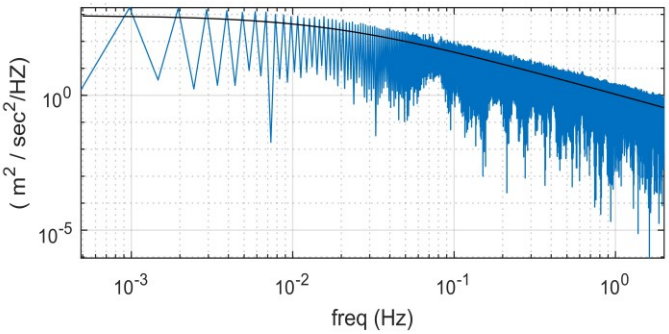

(d) PSD function at point 1

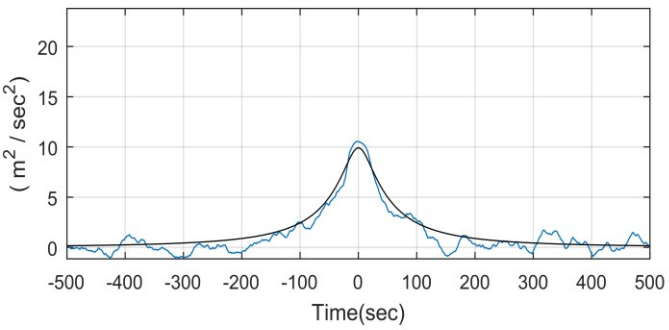

(e) cross-correlation function at points 1 and 9

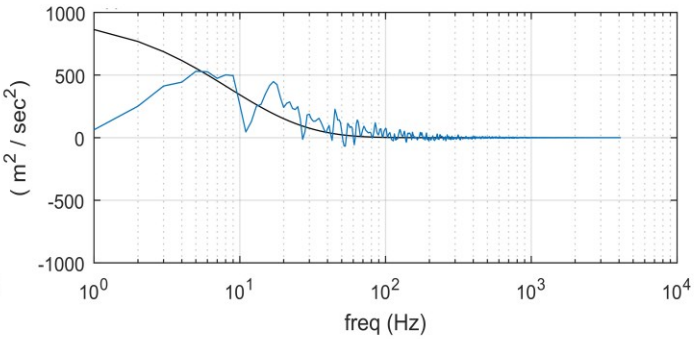

(f) cross-PSD function at points 1 and 9

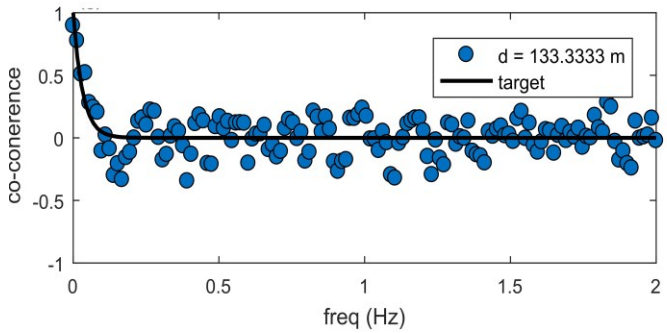

(g) Co-coherence function between points 1 and 9

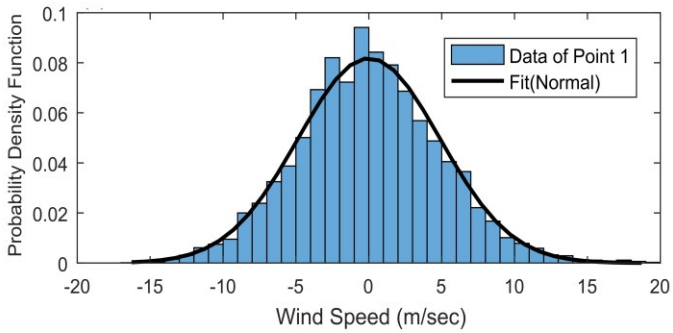

(h) probability density function at point 1

Fig. 11: Outputs of longitudinal wind speeds and their statistical analysis using SR-method.

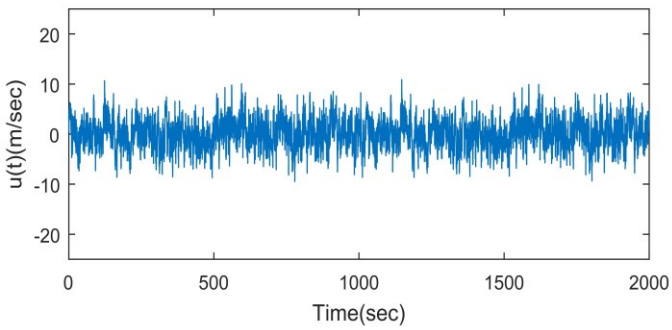

(a) Cross velocities at point 1

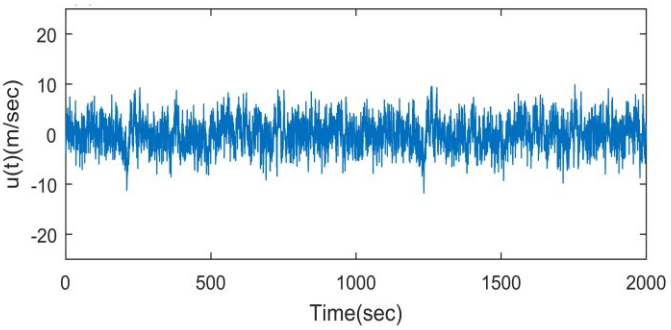

(b) Cross velocities at point 9

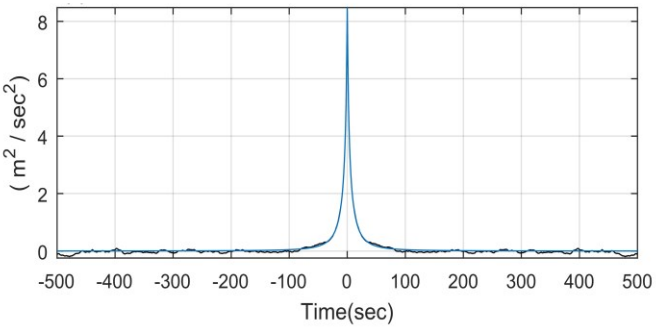

(c) Auto correlation function at point 1

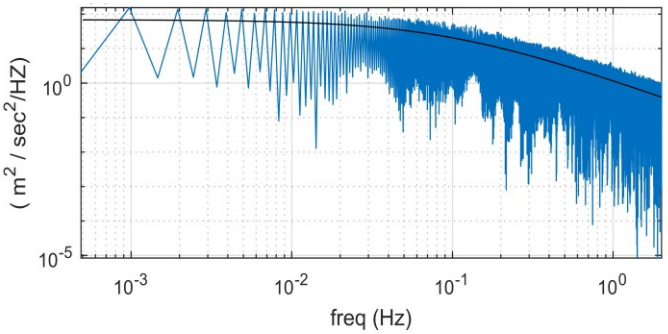

(d) PSD function at point 1

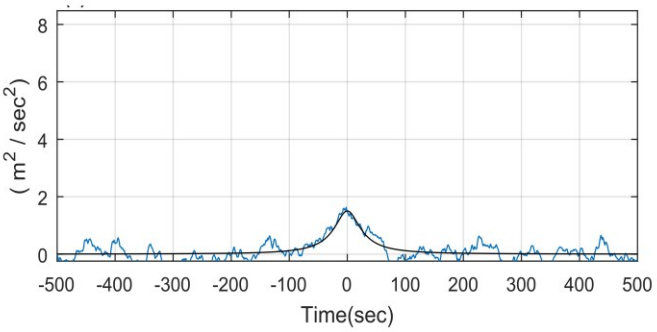

(e) cross-correlation function at points 1 and 9

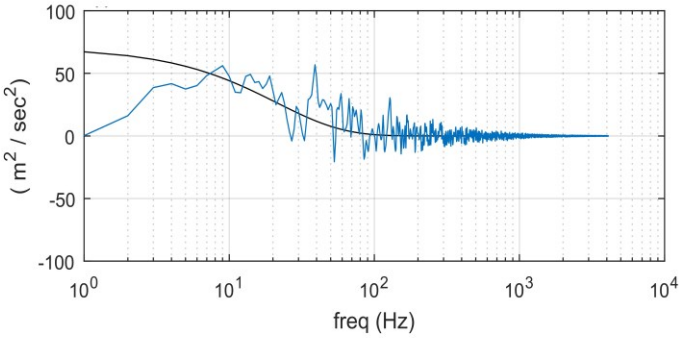

(f) cross-PSD function at points 1 and 9

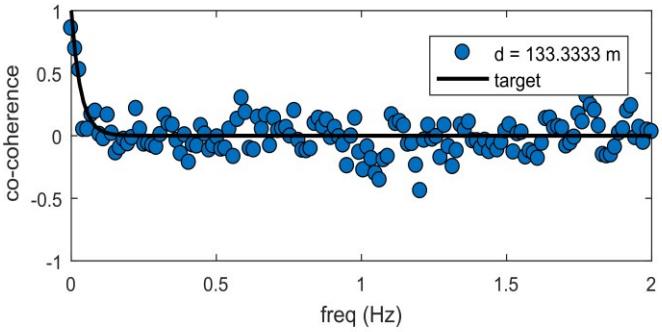

(g) Co-coherence function between points 1 and 9

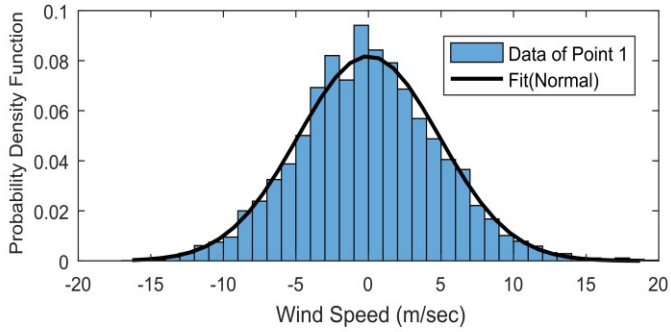

(h) probability density function at point 1

Fig. 12: Outputs of cross wind speeds and their statistical analysis using SR-method.

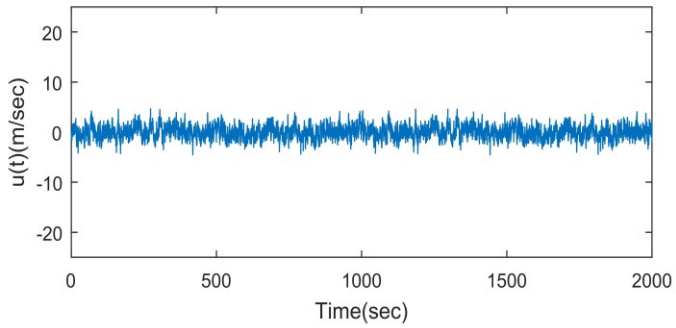

(a) Vertical velocities at point 1

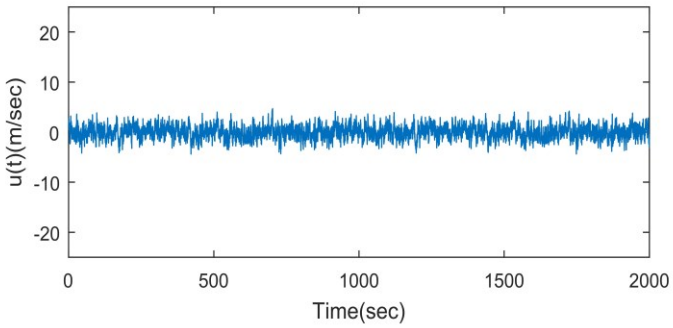

(b) Vertical velocities at point 9

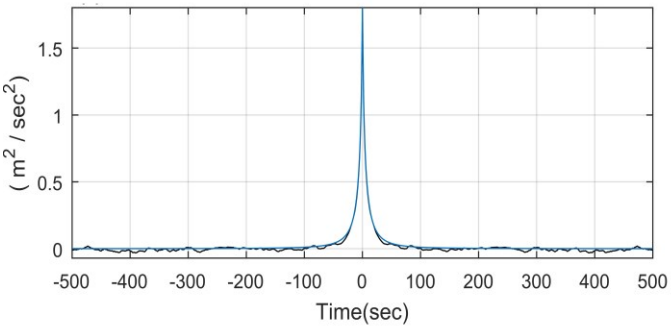

(c) Auto correlation function at point 1

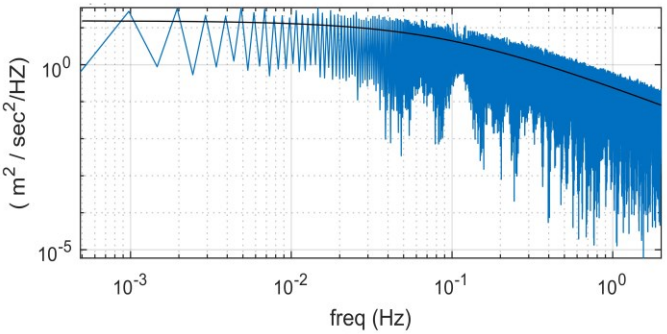

(d) PSD function at point 1

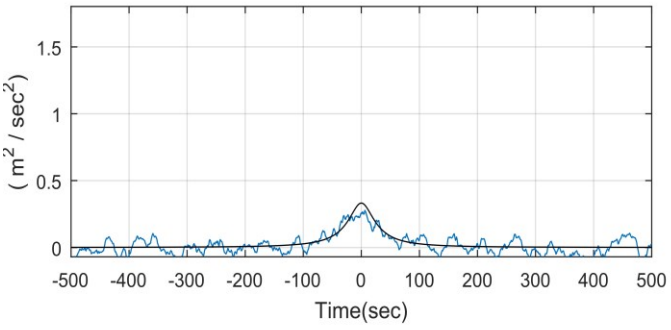

(e) cross-correlation function at points 1 and 9

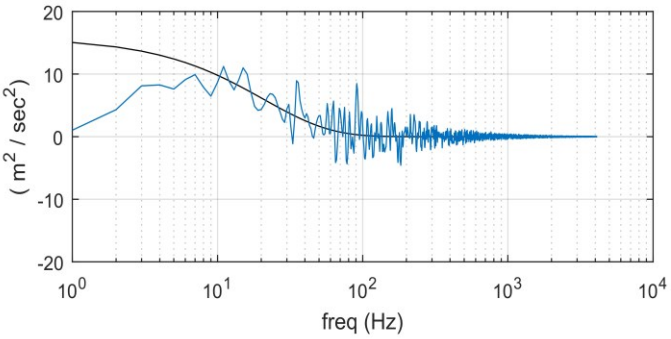

(f) cross-PSD function at points 1 and 9

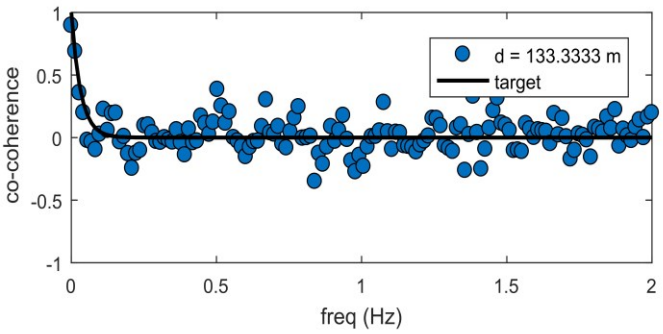

(g) Co-coherence function between points 1 and 9

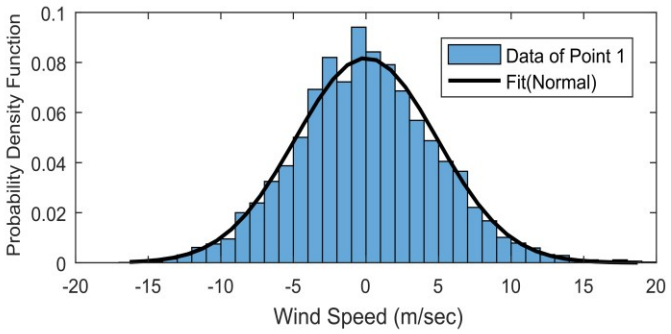

(h) probability density function at point 1

Fig. 13: Outputs of vertical wind speeds and their statistical analysis using SR-method.

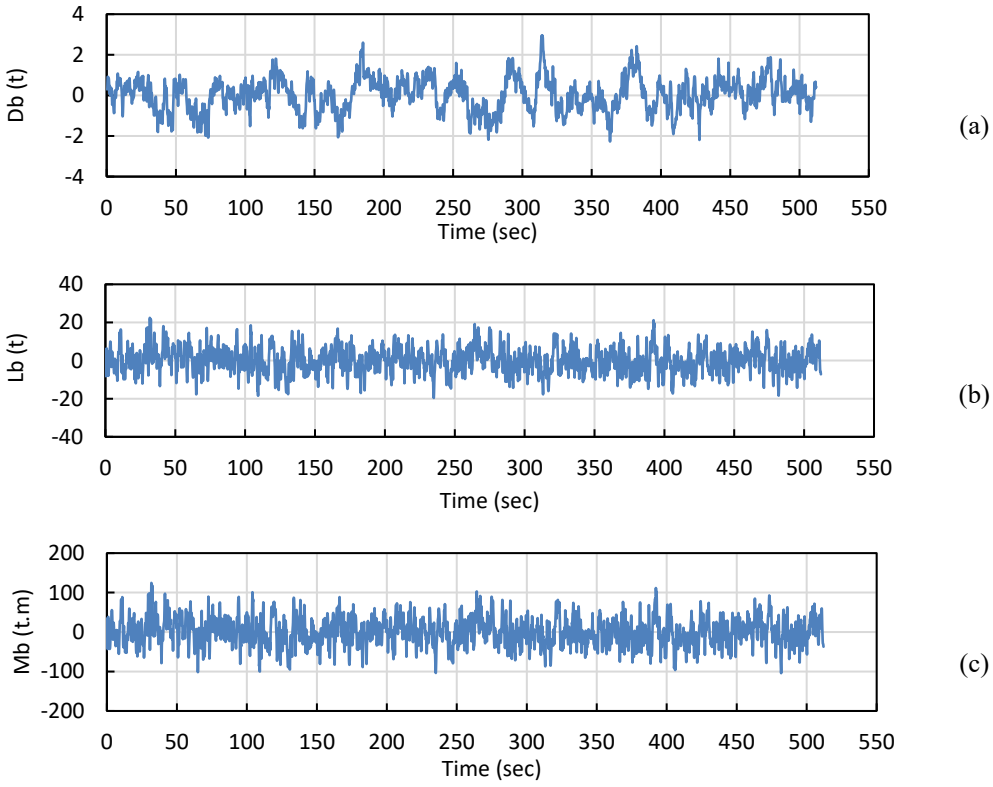

Fig. 14: Buffeting force (unit) on element at center of main span $\boldsymbol{U_{10} = 30\ m/sec}$: (a) Drag force; (b) Lift force; (c)Moment.

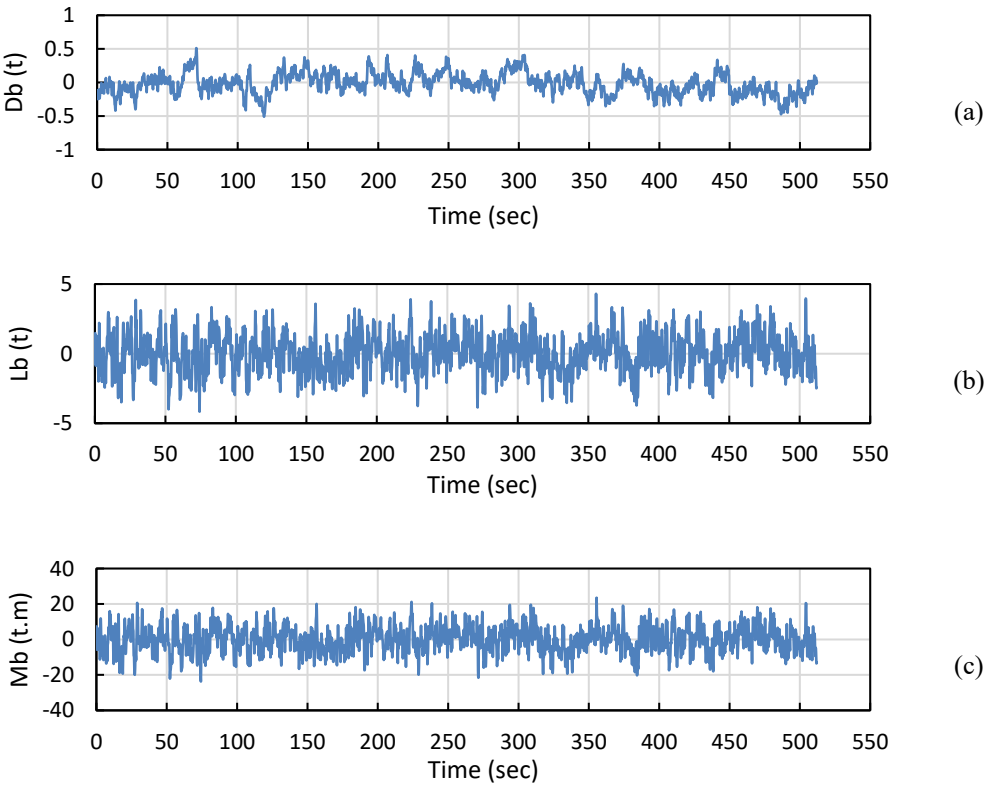

Fig. 15: Buffeting force (sears) on element at center of main span $U_{10} = 30\ m/sec$: (a) Drag force; (b) Lift force; (c)Moment.

VII. CONCLUSION

- The proposed simulation methods (AR and SR) showed a good efficiency in generating wind histories of the spatial 3-D fields for longitudinal, cross and vertical turbulent wind. Also, the simulated auto/cross-correlation functions of the simulated wind forces in two methods have good conformity with the target functions.
- SR method shows to be more accurate than the AR method in terms of generating wind histories.
- AR method is quite preferable in terms of memory because it uses fewer computer memory.
- AR method is computationally efficient in terms of reducing the execution time for wind histories.

Notations

u(t)	The stochastic process to be generated
a(t)	The input white noise with zero mean and variance $\sigma_a{}^2$
$\gamma(B)$	The transfer function or filter
$\bar{U}(z)$	The mean wind speed at height z
z_0	The surface roughness length
u_*	The friction velocity
U (10)	The reference mean wind velocity measured at 10 m above ground level
k	von Karman's constant ~ 0.4
L	The lower matrix
n(t)	The random numbers
$N^i(t)$	a random shock having appropriate cross-correlation.
K	The number of histories to be generated
M	The order of AR-filter
Φ_m^{ij}	The autoregressive matrix
$u_j(t)$	The generated time history of wind turbulent component with zero at point j.
$H(f)$	The lower triangular matrix obtained from decomposition of a PSD matrix at each frequency.
$\emptyset_{ml}$	The random phase angles which are uniformly distributed over the interval $[0,2\pi]$
f_{ml}	The double indexing of frequency
Δf	The frequency increment
f_{up}	The upper cutoff frequency at which the values of PSD matrix elements are assumed to be zero
N	The number of studied frequencies
$\theta_{jm}(f_l)$	The complex angle of $H_{jm}(f_l)$
L	is the length of bridge deck
H	The height of pylon
x-axis	The lateral direction that is normal to the deck axis (the main direction)
y-axis	The longitudinal direction that is along the deck axis
z-axis	The vertical direction
u, v, w	The turbulent fluctuations in the lateral (x), longitudinal (y) and vertical direction (z), respectively
D	The separation
f	The natural frequency
ω_{up}	The Upper cutoff frequency
N	Dividing number of frequencies
N_T	Dividing number of times
Δt	Time interval

AUTHORS CONTRIBUTION

M. Naguib	Data analysis and interpretation; Investigation; Software; Supervision; Final approval of the version to be published
Y. Agag	Critical revision of the article; Final approval of the version to be published; Supervision.
A. G. Khedr	Data collection and tools; Data analysis and interpretation; Investigation; Methodology; Software.

REFERENCES

[1] G. Shinozuka, M. and Deodatis, Simulation of stochastic processes by spectral representation, Apply Mech. Rev. 44(4) (1991) 191–203. https://doi.org/https://doi.org/10.1115/1.3119501.

[2] A. Kareem, M.C. McCullough, Numerical Simulation of Wind Effects, in: Adv. Struct. Wind Eng., Springer Japan, Tokyo, 2013: pp. 261–299. https://doi.org/10.1007/978-4-431-54337-4_10.

[3] M. Shinozuka, Simulation of Multivariate and Multidimensional Random Processes, J. Acoust. Soc. Am. 49 (1971) 357–368. https://doi.org/10.1121/1.1912338.

[4] M. Shinozuka, C.-M. Jan, Digital simulation of random processes and its applications, J. Sound Vib. 25 (1972) 111–128. https://doi.org/10.1016/0022-460X(72)90600-1.

[5] J.-N. Yang, Simulation of random envelope processes, J. Sound Vib. 21 (1972) 73–85. https://doi.org/10.1016/0022-460X(72)90207-6.

[6] M. Shinozuka, Digital simulation of random processes in engineering mechanics with the aid of FFT technique(Fast Fourier Transformation), Stoch. Probl. Mech. (1974) 277–286.

[7] M. Shinozuka, R. Levy, Generation, of wind velocity field for design of antenna reflectors, accepted for publication in Eng, Mech. Div. Proc. ASCE. 230 (n.d.).

[8] G. Deodatis, M. Shinozuka, Simulation of Seismic Ground Motion Using Stochastic Waves, J. Eng. Mech. 115 (1989) 2723–2737. https://doi.org/10.1061/(ASCE)0733-9399(1989)115:12(2723).

[9] G. Deodatis, Simulation of Ergodic Multivariate Stochastic Processes, J. Eng. Mech. 122 (1996) 778–787. https://doi.org/10.1061/(ASCE)0733-9399(1996)122:8(778).

[10] Y. Cao, H. Xiang, Y. Zhou, Simulation of Stochastic Wind Velocity Field on Long-Span Bridges, J. Eng. Mech. 126 (2000) 1–6. https://doi.org/10.1061/(ASCE)0733-9399(2000)126:1(1).

[11] Q. Ding, L. Zhu, H. Xiang, An efficient ergodic simulation of multivariate stochastic processes with spectral representation, Probabilistic Eng. Mech. 26 (2011) 350–356. https://doi.org/10.1016/j.probengmech.2010.09.006.

[12] G. Huang, H. Liao, M. Li, New formulation of Cholesky decomposition and applications in stochastic simulation, Probabilistic Eng. Mech. 34 (2013) 40–47. https://doi.org/10.1016/j.probengmech.2013.04.003.

[13] N. Chen, Y. Li, H. Xiang, A new simulation algorithm of multivariate

short-term stochastic wind velocity field based on inverse fast Fourier transform, Eng. Struct. 80 (2014) 251–259. https://doi.org/10.1016/j.engstruct.2014.09.012.
[14] Y. Wu, Y. Gao, A modified spectral representation method to simulate non-Gaussian random vector process considering wave-passage effect, Eng. Struct. 201 (2019) 109587. https://doi.org/10.1016/j.engstruct.2019.109587.
[15] Y. Iwatani, Simulation of multidimensional wind fluctuations having any arbitrary power spectra and cross spectra, J. Wind Eng. 11 (1982) 5–18.
[16] A. Iannuzzi, P. Spinelli, Artificial Wind Generation and Structural Response, J. Struct. Eng. 113 (1987) 2382–2398. https://doi.org/10.1061/(ASCE)0733-9445(1987)113:12(2382).
[17] Z. Huang, Z.S. Chalabi, Use of time-series analysis to model and forecast wind speed, J. Wind Eng. Ind. Aerodyn. 56 (1995) 311–322. https://doi.org/10.1016/0167-6105(94)00093-S.
[18] T. Stathopoulos, K.S. Kumar, A.R. Mohammadian, Design wind pressure coefficients for monoslope roofs: A time series approach, J. Wind Eng. Ind. Aerodyn. 65 (1996) 143–153. https://doi.org/10.1016/S0167-6105(97)00031-7.
[19] L. Facchini, The numerical simulation of Gaussian cross-correlated wind velocity fluctuations by means of a hybrid model, J. Wind Eng. Ind. Aerodyn. 64 (1996) 187–202. https://doi.org/10.1016/S0167-6105(97)00004-4.
[20] Y.Q. Li, S.L. Dong, Random wind load simulation and computer program for large-span spatial structures, Spat. Struct. 7 (2001) 3–11.
[21] P. Poggi, M. Muselli, G. Notton, C. Cristofari, A. Louche, Forecasting and simulating wind speed in Corsica by using an autoregressive model, Energy Convers. Manag. 44 (2003) 3177–3196. https://doi.org/10.1016/S0196-8904(03)00108-0.
[22] H. A. Buchholdt, Structural dynamics for engineers, Thomas Telford, London, 1997.
[23] G.E.P. and J. Box, Time Series Analysis: Forecasting and Control, Holden Day, San Francisco, 1977.
[24] Y.-L. Xu, Wind Effects on Cable-Supported Bridges, first, John Wiley & Sons Singapore Pte. Ltd., Singapore, 2013. https://doi.org/10.1002/9781118188293.
[25] J.C. Kaimal, J.C. Wyngaard, Y. Izumi, O.R. Coté, Spectral characteristics of surface-layer turbulence, Q. J. R. Meteorol. Soc. 98 (1972) 563–589. https://doi.org/10.1002/qj.49709841707.
[26] R.H. Simiu, E. and Scanlan, Wind Effects on Structures: Fundamentals and Applications to Design, 3rd edn, John Wiley & Sons., Inc., New York., 1996.
[27] A.G. Davenport, The dependence of wind load upon meteorological parameters. Proceedings of the International Research Seminar on Wind Effects on Buildings and Structures, (1968) 19–82.
[28] Iannuzzi I .A., Response of Guyed Masts to Simulated wind, The Polytechnic of Central London, London, U.K., 1987.
[29] M. Naguib, Buckling strength and dynamic response of guyed towers, Mansoura University, 1989.
[30] M.C.H. Hui, Q.S. Ding, Y.L. Xu, Buffeting Response Analysis of Stonecutters Bridge, HKIE Trans. 12 (2005) 8–21. https://doi.org/10.1080/1023697X.2005.10667998.

Title Arabic

المحاكاة العدديه لأحمال الرياح المتعصفة على الكبارى (الملجمة) ذات الكابلات.

Abstract Arabic

الطرق العددية هي أداة معتمدة على نطاق واسع لمحاكاة تاريخ الرياح. الطريقة الاكثر دقة هى اختبار نفق الرياح ، ولكنها ليست الإختيار الأكثر اقتصادية. لذلك ، تهتم الكثير من الأبحاث بتطوير تلك الطرق لتكون أكثر دقة وقابلة للتطبيق ولتوفير وقت الحل. يهتم هذا البحث بمقارنة طريقتين لمحاكاة العمليات الغاوسية العشوائية الثابتة وهذه الطرق هي طريقة الانحدار الذاتي (AR)وطريقة التمثيل الطيفي(SR). لتنفيذ تقنية المحاكاة للطريقتين، تم عمل برنامج باستخدام MATLAB. وتم تطبيق كلتا الطريقتين باستخدام جسر مثبت بالكابلات (كوبري ملجم) يبلغ طوله ٦٧٠ مترًا كطول رئيسى لدراسة مجموعة من النقاط على طول سطح الجسر.وقد تم عمل مقارنة بين النتائج التي تم الحصول عليها لكل من الطريقتين. وتم حساب الخصائص الإحصائية لمقارنة وتقييم نتائج كلتا الطريقتين بدقة. تم ملاحظة أن دوال الارتباط الذاتى والمتبادل بين القيم المحاكاة لقوى الرياح المحاكاة بالطريقتين متوافقة بشكل جيد مع الدوال المستهدفة. بخلاف ذلك ، تكون طريقة SR أكثر دقة من طريقة AR ، لكن الوقت المنفذ بطريقة SR أكثر من طريقة AR. بعد ذلك تم اختيار الطريقة المناسبة للكباري المثبتة بالكابلات وتم تطبيقها على الجسر محل الدراسة لتوليد قوى الرياح المتعصفة عليه.